The 4th Joint International Conference on Multibody System Dynamics
May 29 – June 2, 2016, Montréal, Canada

Dual-Triangular Remote Centre of Motion Mechanism With Cable Transmission

Shao Liu[1], Binbin Chen[1], Stéphane Caro[2], Sébastien Briot[2] and Chao Chen[1]

[1]*Department of Mechanical and Aerospace Engineering, Monash University, {shao.liu, chao.chen, binbin.chen}@monash.edu*
[2]*IRCCyN, {stephane.caro, sebastien.briot}@irccyn.ec-nantes.fr*

ABSTRACT *The remote centre of motion (RCM) mechanisms are increasingly used to develop robotic surgical systems. Currently, parallelogram-based planar RCM mechanism are often combined with single revolute joint to deliver the two degrees of freedom (DOFs) required in the minimally-invasive surgical applications. However, parallelogram-based planar RCM mechanisms encounter issues associated with device footprint, which compromise optimal surgical functioning. The dual-triangular linkage (DT-linkage) with RCM is proposed in the attempt to replace the parallelogram-based linkage and resolve the footprint issue. This paper presents the work on the design and static analysis of cable-based auxiliary mechanism for DT-linkage. The aim is to achieve backlash-free and singularity-free mechanical constraint, such that the ROM of the original DT-linkage can be doubled without expanding the device footprint. A constraint approach is conducted to solve for the force within the cable sections. The analytical solution at singular configuration indicates tension in all cable sections hence proved the functioning of the cable constraint. By utilising the QR decomposition, the numerical solution of minimum required cable stiffness is also calculated from the constraint approach.*

1 Introduction

To promote safety, robotic surgical systems include remote center of motion (RCM) property as one of their central function [1], which allows the manipulators to be pivoted around their incision ports. The RCM function is normally achieved by the implementation of RCM mechanisms. By definition, if a link of the mechanism can rotate around a fixed point distal from the mechanism, while there is no physical revolute joint at the fixed point, the mechanism is referred to as an RCM mechanism [2, 3].

A remote center (RC) can be constrained virtually or mechanically [4]. Mechanical RCM mechanisms are more reliable and considered suitable for clinical applications [2]. Mechanical RCM mechanisms that generate single RC and are applied on surgical robots have been well documented, which include isocentres [5], circular tracking arcs [6, 7], parallelograms [8, 9, 10, 11, 12, 13], synchronous transmissions [14] and spherical linkages [15]. There are also RCM mechanisms that generate multiple RCs [16], but their applications in minimally-invasive surgeries (MIS) are not yet explored.

Surgical manipulations through RC require two rotational and one translational degrees of freedom (DOF) to fully define the position of the end-effector inside the patient's body. In practice, the two rotational DOFs are often generated by combining a one-DOF planar RCM mechanism with a single revolute joint [2], where the one-DOF RC is located on the axis of the revolute joint. A mechanism that generates the translational DOF is then attached to the output link of the planar RCM mechanism.

Such approach results in fully decoupled mechanism that has reduced complexity in control, promoted level of confidence in safety as well as rapid and intuitive manual positioning of the entire mechanism or individual DOF [17]. Alternatively, by trading off the decoupled motion [18] or the compact transverse dimension of the mechanism [19], the translational DOF can be achieved also by the planar RCM mechanisms, such that no additional mechanical structure is required.

Parallelogram is selected as the planar RCM mechanism in many RCM robotic surgical systems based on the aforementioned approach [2], including the most widely-deployed da Vinci series [10, 20, 21]. In addition, it can also be used to generate the translational DOF [22]. However, most of the issues associated with a parallelogram-based linkage (PB-linkage) are due to its footprint, which is closely related to the output joint of the parallelogram [23]. For RCM mechanisms based on revolute joint with planar RCM mechanisms, the device footprint in 3D is defined by rotating the enclosed area formed by boundary the planar RCM mechanism and the axis of the revolute joint. In MIS, the presence of the output joint close to the RC leads to larger device footprint within the incision port. Thus the chance of interference with neighbouring robotic surgical arms or human surgeons is increased. On the other hand, pushing the output joint away from this region requires a longer output link, hence expands the geometry of the parallelogram as well as the overall device footprint.

More significantly, for the RCM mechanisms with decoupled translational DOF, the use of PB-linkage introduces negative impact on the integration of the translational mechanism [23]. To achieve the decoupled motion, the translational mechanism is forced mounted directly onto the output link of the PB-linkage, which is operated within the region near the RC. Therefore it further increases the device footprint as well as the chance of interference. Poor access for bedside assistance [21] and larger chance of collisions or restricted workspace for individuals have been reported, hence prevent optimal surgical functioning [24].

To avoid the issue associated with device footprint near the RC while maintaining the fully-decoupled motion and small overall device footprint, a novel planar RCM mechanism, named the dual-triangular linkage (DT-linkage), was proposed to replace the PB-linkage. The DT-linkage is developed based on virtual four-bar linkage, with two parallelograms to constrain the motion. The mathematical proof of RCM function as well as a passive prototype built for validating the design concept are presented in [4]. Auxiliary mechanisms are introduced into the second prototype [23], which removes the singularity of the DT-linkage and achieves doubling of range of motion (ROM) without changing the dimension and footprint of the mechanism.

Several issues are discovered on the linkage and gear-train based auxiliary mechanisms in the second prototype. Most significantly, the backlash introduced by the gear-train compromises the positioning accuracy and stiffness of the system [23]. Apart from that, the parallelograms in both prototypes occupy additional space in between the input joint and the RC. Such design conflicts with the design concept of minimising the device footprint near the RC. Therefore it is desired that alternative constraining mechanisms are designed to remove the backlash and reduce the footprint of the planar DT-linkage.

Cable transmission provides backlash-free transmission. In addition, cable transmission can replace the linkage-based parallelograms to reduce device footprint. An example showing such reduction in footprint is the widely deployed da Vinci surgical manipulators, from the linkage-constrained original model to the belt-constrained da Vinci S/Si models [25]. Therefore the new constraining mechanisms are designed based on cable transmission.

This paper presents the work on the design, proof of functioning and load analysis of the cable-based auxiliary mechanism for the DT-linkage. Section 2 briefs the structure, singularity and existing auxiliary mechanisms of the DT-linkage. Section 3 presents the design of the cable transmission. Section 4 proofs the functioning of the cable system mathematically. Section 5 covers the analysis to determine the minimum required cable stiffness with respect to a given overall stiffness of DT-linkage.

2 The Dual-Triangular Linkage and Auxiliary Mechanisms

Details regarding the mechanical structure and mathematical proof of functioning of the DT-linkage are described in [4, 23], along with the singularity analysis and the corresponding design of the auxiliary mechanisms for overcoming singularity. For completeness of this paper, the key information is summarised below.

2.1 The unconstrained DT-Linkage

The concept of unconstrained DT-linkage is shown in Fig. 1, which is based on two pairs of similar triangles: one pair of OFG and OAC and another pair of OHG and OEC. The outer shape of the DT-linkage, which is the virtual four-bar linkage ACEO, adopts 2K-SLLS structure as classified in [26]. In such structure 2 stands for two link

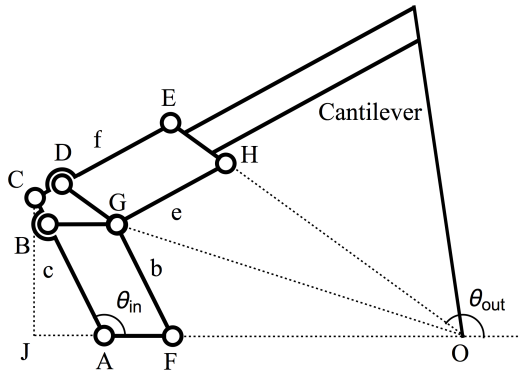

Fig. 1: Conceptual design using the DT-linkage

lengths, K stands for the symmetry kite shape, SLLS (short-long-long-short) stands for the configuration of links in which the links with the same length are adjacent to each other, while the ground and output links being the longer ones. By having shorter input and connector links, the SLLS arrangement ensures that the output joints (Joints E and H) stay relatively distal from the RC, at a given distance between the input joint (Joint A) and the RC. Such feature is the key to materialise the design concept of DT-linkage, as keeps the major linkages away from the RC, leaving more collision-free space for the neighbouring robotic surgical arms or human surgeons to occupy.

Links AF (AO), AC, CE and EH (EO) are the ground, input, connector and output links, respectively. Point O is the RC. Links BG, FG, DG and GH belong to Parallelograms ABGF and DEHG, which enforce the similarity of the triangles. The straight link that is rigidly connected to output link EH represents the cantilever that connects the DT-linkage and the surgical tool. Such cantilever is the only link from the entire DT-linkage, which is relatively close to the RC.

With a given distance between Joint A and O, the geometry of the DT-linkage is fully defined by two parameters, ν and r, expressed mathematically as

$$\nu = \frac{c}{\overline{AO}} \tag{1}$$

and

$$r = \frac{c}{b} = \frac{f}{e} \tag{2}$$

where

$$\begin{aligned} c &= f \\ b &= e \end{aligned} \tag{3}$$

Where c, b, f and e are the lengths of Links AC, FG (AB), CE and GH (DE), respectively. Parameter ν defines the length of the input and connector links when distance AO is given. Parameter r is a constant greater than 1, and it defines the width of Parallelograms ABGF and CEHG. The larger the magnitude of r, the wider the parallelograms are, hence occupies more space in between the input joint and the RC.

Referring to Fig. 1, The input-output function of the RCM mechanism can be found readily as

$$\begin{aligned} \theta_{out} =& \pi - 2\arctan\frac{\overline{CJ}}{\overline{JO}} \\ =& \pi - 2\arctan\frac{\overline{AC}\sin\theta_{in}}{\overline{AO} - \overline{AC}\cos\theta_{in}} \end{aligned} \tag{4}$$

where θ_{in} and θ_{out} are the input angle measured from Link AO to AC counter-clockwise and the output angle measured from AO to OE counter-clockwise, respectively.

The limit in ROM, i.e. the minimum θ_{out}, is reached at the fully stretched-out configuration where Links AC and CE are in-line with each other. The other limit in ROM is the configuration where all the links are coincident

with the ground axis behind the input joint. The corresponding θ_{out} is 180 degrees. Details regarding such configuration are given in the next sub-section. At the fully stretched-out configuration, Link AC is perpendicular to Line CO, thus the ROM is written as

$$ROM = 2\arcsin(v) \tag{5}$$

2.2 Singularity Analysis and Existing Auxiliary Mechanisms

There are two fully stretched-out configurations on a DT-linkage, at above and below the ground axis, respectively. Thus the theoretical ROM is limited in between the two fully stretched-out configurations as

$$ROM = 4\arcsin(v) \tag{6}$$

Equation (6) indicates that the ROM is doubled comparing to the unconstrained case, and without expanding the dimension of the linkage and hence the device footprint. To achieve so, the DT-linkage must be able to pass through the singular configuration, where all the links are coincident with the ground axis.

The singularity of the unconstrained DT-linkage is sourced from both the virtual four-bar linkage ACEO and the Parallelograms ABGF and DEHG. Since the four-bar linkage and the parallelograms encounter singularity at the fully-folded configuration, such configuration is also the singular configuration of the DT-linkage. To overcome the singularity, the four-bar linkage and the parallelograms must be constrained simultaneously. Therefore, one auxiliary mechanism is designed for each of the four-bar linkage and the parallelogram, respectively.

For four-bar linkage, there are two possible configurations after passing the singular configuration, which are

$$\angle ACE = 0 \tag{7}$$

and

$$\angle ACE = 2\angle OCA \tag{8}$$

Where the former case is an undesired configuration where the output link stays overlapped with the ground axis regardless of the input angle. To overcome the singularity, constraint as shown in Eqn. (8) is enforced.

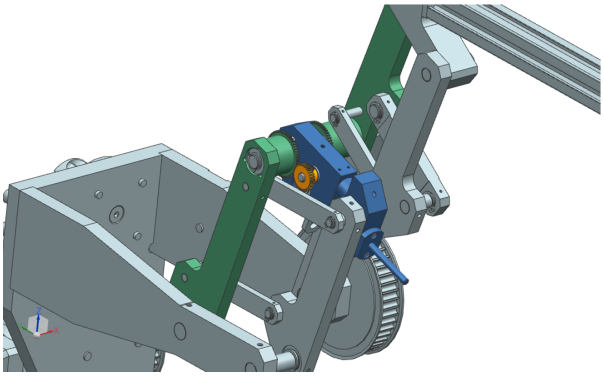

Fig. 2: Configuration of auxiliary mechanism for four-bar linkage - right view

The design of auxiliary mechanism for four-bar linkage is shown in Figs. 2 and 3. The figures are the right and left views, respectively. The auxiliary mechanism synchronises the angular positions of Links AC and CE (coloured green, lower and upper, respectively) with respect to the centre line of the four-bar linkage, CO. To accommodate for the change in length between Joints C and G, where CG is coincident with CO, a translational joint is introduced. Link group CG is coloured blue in the figures. The synchronisation of angular positions is achieved through a gear-train with five gears. Gears 1 and 5 (both green) are rigidly attached to Links AC and CE,respectively. Gears 2 to 4 rotate freely on link group CG. Gear 2 (orange, visible in Fig. 2) measures $\angle OCA$. Gear 3 (orange, visible in Fig. 3) is rigidly connected to and rotates with Gear 2, in order to reach Gear 4 (red, visible in Fig. 3) on the other side of link group CG. Gear 4 measures $\angle OCE$. It engages with Gears 3 to ensure the two angles stay in directions, thus achieves Eqn. (8).

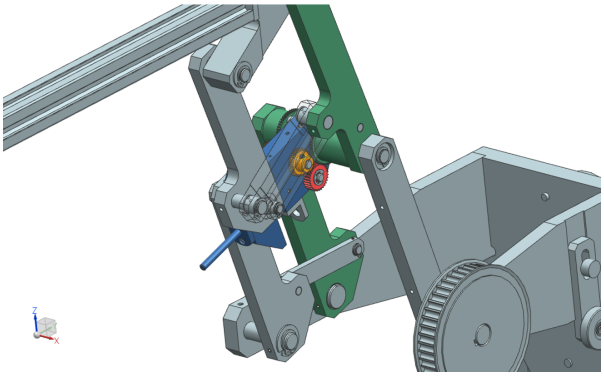

Fig. 3: Configuration of auxiliary mechanism for four-bar linkage - left view

For Parallelograms ABGF and DEHG, two auxiliary parallelograms are introduced, respectively. Parallelograms AA'F'F and DD'G'G are rigidly attached to and angularly displaced from Parallelograms ABGF and DEHG, respectively, as shown in Fig. 4. Each pair of original and auxiliary parallelograms are not in the singular configuration simultaneously, hence are constraining each other to achieve singularity-free structure.

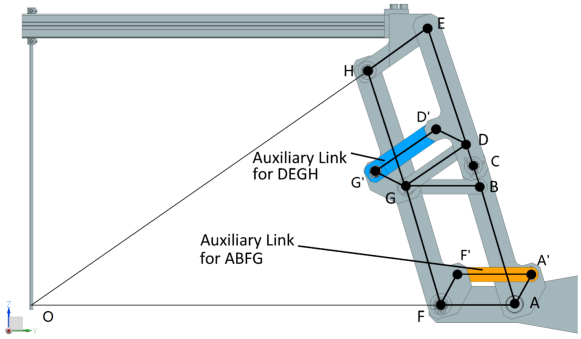

Fig. 4: Configuration of parallelograms with auxiliary links

3 Design of Cable System

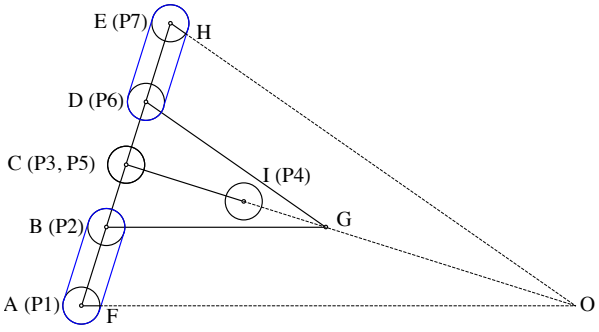

Fig. 5: Configuration of Loop PL and PU

The cable system consists of a translational joint and seven pulley that form three cable loops. Figs. 5 shows the two cable loops, PL and PU, for replacing Parallelograms ABFG and DEHG, respectively. Figs. 6 and 7 illustrate two halves of the cable loop that constrains the virtual four-bar linkage. The ones in Figs. 6 and 7 are named

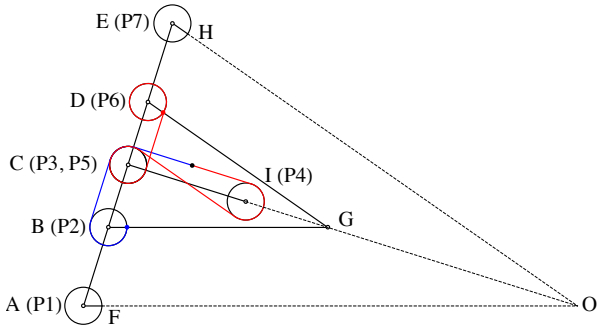

Fig. 6: Configuration of cable loop for four-bar linkage - Section FB1

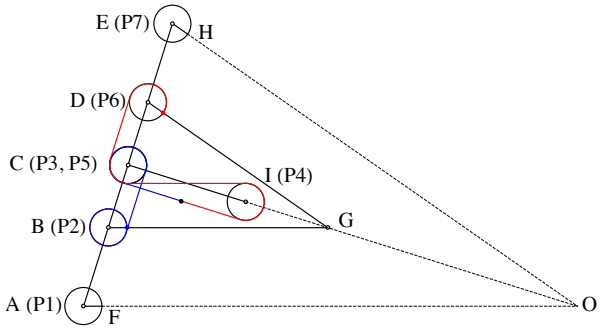

Fig. 7: Configuration of cable loop for four-bar linkage - Section FB2

Section FB1 and FB2, respectively. Each half of Loop FB constrains the DT-linkage in one direction of its motion. Sections FB1 functions when DT-linkage moves from the fully stretched-out configuration below the ground axis to the one above, while Section FB2 functions in the opposite direction. Sections FB1 and FB2 join at the blue and red dots on pulleys at B and D, respectively. Note that for better illustration of structure, the dimension of four-bar linkage BCDG is much larger the one on existing prototypes. The radius of pulleys, R, applies to all the pulleys and is independent of the dimensions of links.

The translational joint is represented as Link Group CIG in the figures. The translational joint is located in between Joints I and G, thus the distance between Joints C and G is fixed. Pulleys 1, 2, 6, and 7 are mounted at Joints A, B, D and E, respectively, and are rigidly attached to Links AF, BG, DG and EH, respectively. Pulleys 3 and 5 are mounted at Joint C and can rotate freely. Pulleys 4 is mounted at Point I on diagonal link group CIG and rotates freely.

In Figs. 6 and 7, Sections FB1 and FB2 are further divided into two subsections, coloured blue and red, respectively. The blue subsection contains Pulleys 2 and 3, while the red subsection contains Pulleys 4 to 6. The travel distances of the ends of the blue and red subsections (at the junction where two subsections connect) are associated with Angles $\angle GBC$ and $\angle BCG$, and Angles $\angle GDC$ and $\angle DCG$, respectively. Assuming that the DT-linkage stay in the desired configurations, the travel distances of the ends of subsections should be identical, and vice versa. In this case the possibility of Eqn. (7) is eliminated, and the virtual four-bar linkage is fully-constrained.

To simplify the describe on position of pulleys in the mathematical model, the following lengths are assigned

$$L_1 = \overline{AC} = \overline{CE} = v\overline{AO} \tag{9}$$

$$L_2 = \overline{AB} = \overline{DE} = \frac{L_1}{r} \tag{10}$$

$$L_3 = \overline{AF} = \overline{BG} = \overline{DG} = \overline{EH} = (1 - \frac{1}{r})\overline{AO} \tag{11}$$

4 Static Analysis for Proof of Functioning of Cable System

The functioning of a cable system lies on the tension in cable. For proving the functioning of cable-based auxiliary mechanism, it is essential to prove that the cable sections in between all pair of pulleys are in tension. In the static analysis below, it is assumed that the cable is inextensible and there is no slip between the cable and the pulleys.

4.1 The Constraint Approach

A constraint approach described in [27] is utilised to determine the directions of forces within the cable sections. To start with, the dynamics of a constrained physical system is described as [28]

$$Q_i = Q_c + Q_e \tag{12}$$

Where Q_i, Q_c and Q_e are the generalised inertia, constraint and external forces applied on the generalised coordinates q, respectively. The generalised constraint force Q_c applied on q is related to the mechanical constraints of the systems through

$$Q_c = -C_q^T \lambda \tag{13}$$

Where λ is the Lagrange multiplier, which represents the generalised constraint force acting along the mechanical constraints. C_q is the derivative of the constraint vector c_q with respect to the generalised coordinates q, which is

$$C_q = \frac{\partial c_q}{\partial q} \tag{14}$$

Assuming that c_q and q have dimensions of m and n respectively, the dimensions of Q_c, C_q and λ are $n \times 1$, $m \times n$, and $m \times 1$, respectively.

In static analysis, the generalised inertia force Q_i vanishes. Therefore, combining Eqns. (12) and (13) gives

$$Q_e = C_q^T \lambda \tag{15}$$

or equivalently

$$\begin{aligned} Q_{ei} &= C_{qi}^T \lambda \\ Q_{ed} &= C_{qd}^T \lambda \end{aligned} \tag{16}$$

Where Q_{ei} and Q_{ed} are the generalised external forces applied on q_i and q_d, respectively. C_{qi} and C_{qd} are the derivative matrices determined using q_i and q_d, respectively. Given the generalised external forces Q_e, Eqn. (15) is used to determine the generalised constraint force λ acting along the mechanical constraints.

The direction of such constraint force is dependent on the way in which the constraint equation c_q is written in. An example is given below. Consider an arbitrary constraint equation that is defined as

$$c_q = p_a - p_b \tag{17}$$

Where p_a and p_b are the physical quantities of Bodies A and B, respectively, which are used to construct the constraint equation. In this case the λ determined using such constraint equation is the generalised constraint force acting on Body B by Body A. In the opposite case, if the positions are p_a and p_b are swapped in Eqn. (17), λ will give the generalised constraint force acting on Body A by Body B. To determine the direction of force in between each pair of pulleys, one constraint equation for each pair of pulleys must be obtained.

4.2 Generalised Coordinates q

To fully describe the cable-constrained linkage and derive the constraint equations for cable, twelve generalised coordinates are selected. The independent generalised coordinate is the actuator input rotation of Link AC. The dependent generalised coordinates include the angles of pulleys and links, the distances between joints and the positions of joints.

q	Definition	Reference
θ_1	angle of Link AC	positive ground axis
θ_2	angle of Pulley 2 and Link BG	Link AC along direction AC
θ_3	angle of Pulley 3	Link AC along direction AC
θ_4	angle of Pulley 4	Link CG along direction CG
θ_5	angle of Pulley 5	Link CG along direction GC
θ_6	angle of Pulley 6 and Link DG	Link CE along direction CE
θ_7	angle of Pulley 7 and Link EH	Link CE along direction CE
θ_8	angle of Link CG	Link AC along direction AC
θ_9	angle of Link CE	Link CG along direction GC
L_{CG}	length of Link CG	n/a
x_H	horizontal position of joint H	Joint A
y_H	vertical position of joint H	Joint A

Tab. 1: Link paths for Joints G and H

The generalised coordinates are listed in Table 1. All the angles are measured in the counter-clockwise direction. The 'Reference' column lists the datums which the generalised coordinates are measured with respect to. The references for all the pulley or link angles are selected as the previous links they are attached to, respectively, where the term previous is defined with respect to the direction from Joint A to Joint H of the DT-linkage.

4.3 Constraint Equations and Constraint Matrix

There are two sources of constraint equations in the cable-constrained DT-linkage, leading to twelve constraint equations for each direction of motion of the DT-linkage. The first one is the constant cable length in between the pulley pairs. The second one is the joint position derived from different links paths.

4.3.1 Constraint Equations from Cable

To reduce the amount of calculations, only the cable sections that are expected to be in tension are studied for each direction of motion of the DT-linkage. Six constraint equations are obtained for seven pulleys, including one each from Loops PL and PU, respectively, and four from Section FB1 or FB2 depending on the direction of motion.

To derive the constraint equation for a pair of pulleys, the cable connecting the pulleys is separated at an arbitrary position in the middle. The off-pulley (not wrapped on pulley) lengths of the two separated cable sections change corresponding to the rotations of the pulleys they are connected to, respectively. The sum of the off-pulley lengths of the two cable sections is a constant, as the distance between the pulleys is constant. Therefore, the rotations of the pulleys, which are two generalised coordinates, are related to each other in one constraint equation. Such constraint equation is derived below.

Consider the cable connecting two arbitrary pulleys, Pulleys A and B. The two ends of the cable are fixed on Pulleys A and B, respectively. The distance between the pulleys is L. The radius of the pulleys is R. Upon separation, the lengths of the cable sections connected to Pulleys A and B are L_A and L_B, respectively. On Pulley A, the cable ends where the angle is the generalised coordinate θ_A. The cable leaves Pulley A at angle is θ'_A (outlet angle). On Pulley B, the cable starts to wrap on pulley at angle θ'_B (inlet angle), and ends at where the angle is the generalised coordinate θ_B. Generalised coordinates θ_A and θ_B represent the rotations of Pulleys A and B, respectively. The sum of length of Sections A and B that are off-pulley equals the distance between the pulleys, which is expressed mathematically as

$$\big(L_A - (\theta_A - \theta'_A)R\big) + \big(L_B - (\theta'_B - \theta_B)R\big) = L \tag{18}$$

The $(\theta_A - \theta'_A)R$ and $(\theta'_B - \theta_B)R$ terms in Eqn.(18) give the lengths of cable wrapping on Pulleys A and B, respectively. The sequence of subtraction of angles is determined based on direction in which the cable is wrapped on the pulley, in order to obtain a positive cable length. For cable that wraps clockwise on the pulley, the order of subtraction is inlet angle (starts wrapping on pulley) minus outlet angle (leaves pulley). For the counter-clockwise case, the order of subtraction is outlet angle minus inlet angle. In Eqn. (18), it is assumed that the cable wraps on both pulleys in the clockwise direction.

Equation (18) is rearranged into the form of Eqn. (17) for justification of the direction of constraint force as

$$\Big(L - \big(L_B - (\theta'_B - \theta_B)R\big)\Big) - \big(L_A - (\theta_A - \theta'_A)R\big) = 0 \tag{19}$$

The physical meaning of Eqn. (19) is that the off-pulley lengths of Section B, when calculated through two generalised coordinates θ_B (in first bracket) and θ_A (in second bracket), respectively, must be identical. According to the definition of Eqn. (17), Eqn. (19) gives the constraint force applied on the Section A by Section B.

Since L, L_A and L_B are constant, which yield zero when the derivatives are taken for C_q, Eqn. (19) can be simplified as

$$(\theta'_B - \theta_B)R + (\theta_A - \theta'_A)R - L' = 0 \tag{20}$$

Where L' is a constant containing L, L_A and L_B. As mentioned previously, the order of subtraction in $(\theta'_B - \theta_B)$ and $(\theta_A - \theta'_A)$ can vary independently, according to the directions in which the cable wraps on the individual pulleys. Equation (20) is the constraint equation for Pulleys A and B. When all constraint equations are put together into the constraint vector c_q and solved, the corresponding element of such constraint equation in λ should be positive if the cable between Pulleys A and B is in tension.

To construct the pulley constrain equations with Eqn. (20), three angles need to be determined for each pulley: the inlet and outlet angles, and the generalised coordinate θ. The generalised coordinate θ lies in between the inlet and outlet angles and represents the rotation of the pulley. The inlet and outlet angles of a pulley are measured from the same reference as that of the θ in between them, which is the previous link this pulley is attached to. The values for cable Sections FB1 and FB2 are listed in Tables 2 and 3, respectively. In the tables, the column 'Direction' refers to the direction of cable wrapping on the pulleys, CW for clockwise and CCW for counter-clockwise.

Pulleys	Inlet (rad)	Rotation (rad)	Outlet (rad)	Direction
Pulley 2	n/a	θ_2	$\pi/2$	CW
Pulley 3	$\pi/2$	θ_3	$\theta_8 + \pi/2$	CW
Pulley 4	$\pi/2$	θ_4	$-\pi/2 - \sin^{-1}(2R/L_{CI})$	CW
Pulley 5	$-\pi/2 - \sin^{-1}(2R/L_{CI})$	θ_5	θ_9	CCW
Pulley 6	$-\pi/2$	θ_6	n/a	CCW

Tab. 2: Inlet, outlet and rotation (generalised coordinates) angles of pulleys corresponding to Section FB1

Pulleys	Inlet (rad)	Rotation (rad)	Outlet (rad)	Direction
Pulley 2	n/a	θ_2	$-\pi/2$	CCW
Pulley 3	$-\pi/2$	θ_3	$\theta_8 - \pi/2$	CCW
Pulley 4	$-\pi/2$	θ_4	$\pi/2 + \sin^{-1}(2R/L_{CI})$	CCW
Pulley 5	$\pi/2 + \sin^{-1}(2R/L_{CI})$	θ_5	θ_9	CW
Pulley 6	$\pi/2$	θ_6	n/a	CW

Tab. 3: Inlet, outlet and rotation (generalised coordinates) angles of pulleys corresponding to Section FB2

The values of the three angles for Loops PL and PU are presented in Table 4. When Section FB1 is functioning, the constraint equations are derived from left-hand half of Loop PL and the right-hand half of Loop PU. In the

contrast, when Section FB2 is functioning, the constraint equations are derived from right-hand half of Loop PL and the left-hand half of Loop PU.

Pulleys	Inlet (rad)	Rotation (rad)	Outlet (rad)	Direction
Pulley 1	$\theta_1 - \pi/2$	0	$\theta_1 + \pi/2$	CW
Pulley 2	$\pi/2$	θ_2	$-\pi/2$	CW
Pulley 6	$-\pi/2$	θ_6	$\pi/2$	CW
Pulley 7	$\pi/2$	θ_7	$-\pi/2$	CW

Tab. 4: Inlet, outlet and rotation (generalised coordinates) angles of pulleys corresponding to Sections PL and PU

4.3.2 Constraint Equations from Joint Position

The other six constraint equations come from the horizontal and vertical positions of Joints G and H. The general form of such joint constraint equation is given by

$$\begin{aligned} x_{A|2} - x_{A|1} &= 0 \\ y_{A|2} - y_{A|1} &= 0 \end{aligned} \tag{21}$$

Where the subscripts $A|1$ and $A|2$ refer to the positions of an arbitrary joint, Joint A, derived through two different link paths, Paths 2 and 1, respectively. According to the definition of Eqn. (17), Eqn. (21) gives the constraint force applied on the last link of Path 1 by the last link of Path 2. The link paths for Joints G and H are summarised in Table 5. Note that for Joint H, the generalised coordinates x_H and y_H serve as the second link path to form the constraint equations.

Joints	Path 1	Path 2
G	Links AB-BG	Links AC-CG
G	Links AB-BG	Links AC-CD-DG
H	Links AC-CE-EH	x_H and y_H

Tab. 5: Link paths for Joints G and H

4.3.3 The Constraint Vector c_q and Constraint Matrix C_q

The constraint vector c_q is fully constructed by combining the constraint equations given by Eqns. (20) and (21), in combined with the parameters presented in Tables 2, 3, 4 and 5. The sequence of the elements are constraint equations from cable Sections FB (four equations), then Loops PL and PU (two equations), followed by the constraint equations from Joints G and H (six equations in the same sequence as presented in Table 5). The c_q corresponding

to the upward direction of motion of DT-linkage (Section FB1 functioning) is

$$c_{q1} = \begin{bmatrix} R(\theta_2-\theta_3)+L'_{23} \\ R(\theta_3-\theta_4-\theta_8)+L'_{34} \\ R(\theta_4+\theta_5)+L'_{45} \\ R(-\theta_5+\theta_6+\theta_9)+L'_{56} \\ -R(\theta_1+\theta_2)+L'_{12} \\ R(\theta_6-\theta_7)+L'_{67} \\ (L_1-L_2)c_1-L_3c_{12}+L_{CG}c_{18} \\ (L_1-L_2)s_1-L_3s_{12}+L_{CG}s_{18} \\ (L_1-L_2)(c_1-c_{189})-L_3(c_{12}+c_{1689}) \\ (L_1-L_2)(s_1-s_{189})-L_3(s_{12}+s_{1689}) \\ x_H-L_1c_1+L_1c_{189}+L_3c_{1789} \\ y_H-L_1s_1+L_1s_{189}+L_3s_{1789} \end{bmatrix} \tag{22}$$

The c_q corresponding to the downward direction of motion of DT-linkage (Section FB2 functioning) is

$$c_{q2} = \begin{bmatrix} -R(\theta_2-\theta_3)+L'_{23} \\ -R(\theta_3-\theta_4-\theta_8)+L'_{34} \\ -R(\theta_4+\theta_5)+L'_{45} \\ -R(-\theta_5+\theta_6+\theta_9)+L'_{56} \\ R(\theta_1+\theta_2)+L'_{12} \\ -R(\theta_6-\theta_7)+L'_{67} \\ (L_1-L_2)c_1-L_3c_{12}+L_{CG}c_{18} \\ (L_1-L_2)s_1-L_3s_{12}+L_{CG}s_{18} \\ (L_1-L_2)(c_1-c_{189})-L_3(c_{12}+c_{1689}) \\ (L_1-L_2)(s_1-s_{189})-L_3(s_{12}+s_{1689}) \\ x_H-L_1c_1+L_1c_{189}+L_3c_{1789} \\ y_H-L_1s_1+L_1s_{189}+L_3s_{1789} \end{bmatrix} \tag{23}$$

Where the c and s in the elements of c_q refer to cosine and sine, respectively. The subscripts of c and s represent the summation of θ angles. The L' terms are the constants containing cable lengths.

Once the constraint vectors are obtained, Eqn.(14) is used to obtain the C_q matrix. The dimensions of C_q, C_{qi} and C_{qd} are 12x12, 12x1 and 12x11, respectively.

4.4 Analytical Solution of Cable Tension at Singular Configuration

Equation (15), or equivalently Eqn. (16), is used to determine the generalised constraint force λ along the mechanical constraints, hence the direction of generalised constraint force along each mechanical constraint can be identified to prove the functioning of the cable system.

For the DT-linkage, the generalised external force is

$$Qe = \begin{bmatrix} \tau_1 & 0 & \cdots & 0 & \tau_7 & 0 & \cdots & 0 & F_{Hx} & F_{Hy} \end{bmatrix}^T \tag{24}$$

Where τ_1 is the actuator input torque, τ_7, F_{Hx} and F_{Hy} are the torque and forces applied on Pulley 7 and Joint H, respectively. The dimension of Q_e is 12 by 1, and the sequence of its elements is the same as the sequence of the generalised coordinates q shown in Table 1. The corresponding Q_{ed} contains all the elements in Q_e except for τ_1.

The cable-constraint DT-linkage has twelve generalised coordinates and twelve independent constraint equations, resulting in an over-constrained system. Hence Eqns. (15) and (16) cannot be solved directly for a generalised analytical solution of λ. However, at the singular configuration, one mechanical constraint lapses, leading to fully-constraint system that can be solved directly. Such mechanical constraint comes from link group CIG. Since CIG

contains a translational joint, it is unable to provide any constraint force in the horizontal direction at the singular configuration. The corresponding constraint equation is the ninth element in the c_q vectors in Eqns. (22) and (23).

The two directions of motion of the DT-linkage are simulated by applying vertical forces at Joint H. For upward motion (towards the upper limit in ROM), a negative F_{Hy} is applied and the constraint vector is c_{q1}. For downward motion (towards the lower limit in ROM), a positive F_{Hy} is applied and the constraint vector is c_{q2}.

Since the actuator input torque τ_1 is unknown, Eqn. (16) with Q_{ed} and C_{qd} is used to determine the generalised constraint force λ, instead of the original Q_e and C_q. Q_{ei} which is the input torque, can be recovered afterwards by Eqn. (16) with λ and C_{qi}. An analytical solution of λ is obtained, which contains some dependent generalised coordinates. To eliminate such dependent generalised coordinates, they are represented using the independent generalised coordinate θ_1 as

$$\begin{aligned}
\theta_2 &= -\theta_1 \\
\theta_6 &= \theta_1 + \pi \\
\theta_7 &= \theta_1 + \pi \\
\theta_8 &= -\theta_1 - \tan^{-1}\frac{L_1 s_1}{L_{rc} - L_1 c_1} \\
\theta_9 &= -\theta_1 - \tan^{-1}\frac{L_1 s_1}{L_{rc} - L_1 c_1} \\
L_{CG} &= (1 - \frac{1}{r})\sqrt{(L_1 c_1 - L_{rc})^2 + (L_1 s_1)^2}
\end{aligned} \tag{25}$$

Where L_{rc} is the distance between Joint A and the RC. c_1 and s_1 are the cosine and sine of θ_1, respectively. Note that Eqn. (25) corresponds to the relations at singular configuration only. The analytical solutions of λ at singular configuration are (cable tension elements only, i.e. first six elements)

$$\lambda_1 = \begin{bmatrix}
-\frac{F_{Hy}L_{rc}}{rR} \\
-\frac{F_{Hy}L_{rc}}{rR} \\
-\frac{F_{Hy}L_{rc}}{rR} \\
-\frac{F_{Hy}L_{rc}}{rR} \\
-\frac{\left((1+r)L_1+(-1+r)L_{rc}\right)F_{Hy}L_{rc}}{(L_1+L_{rc})rR} \\
-\frac{(-1+r)F_{Hy}L_{rc}}{rR}
\end{bmatrix} \tag{26}$$

and

$$\lambda_2 = -\lambda_1 \tag{27}$$

for the upward and downward motion of the DT-linkage, respectively. In Eqn. (26), since F_{Hy} is negative and r is greater than 1, all the elements in λ are positive, indicating tension in cable. Similarly, the positive F_{Hy} in Eqn. (27) leads to positive elements. Therefore, the cable sections in between all pulley pairs are proven to be in tension in both direction of motion of the DT-linkage, and hence the singularity-overcoming function of the cable-based auxiliary mechanism is proven.

5 Cable Stiffness Calculation

The minimum required overall stiffness of the system is

$$k = ||\frac{F_{Hy}}{d_{yH}}|| = 1600N/m \tag{28}$$

Where the magnitude of F_{Hy} is 8 N and the maximum allowed d_{yH} is 5 mm. The stiffness of the cable must be sufficient to achieve the overall stiffness. Since the tensions and elongation of cable in between different pulleys

are different, the maximum stiffness must be selected as the minimum design requirement. Such stiffness of the cable is defined as

$$k_{min} = \max ||\frac{\lambda_i}{dL_i}|| \tag{29}$$

Where λ_i is the cable tension in between two pulleys and dL_i is the elongation of cable in between two pulleys. Equation (29) requires the λ_i and dL_i terms to be calculated at all configurations of the DT-linkage.

5.1 Cable Tension

While Eqns (26) and (27) give the analytical solution for λ at the singular configuration, λ cannot be solved directly by Eqn. (15) or (16) at all other configurations of the DT-linkage, due to over-constrained system. Thus for non-singular configurations of the DT-linkage, the numerical solution of λ is calculated through QR decomposition

$$\lambda = Q_1 R_1^{-T} Q_{ed} \tag{30}$$

where

$$\begin{bmatrix} Q_1 & Q_2 \end{bmatrix} \begin{bmatrix} R_1 \\ 0 \end{bmatrix} = \mathrm{QRD}(C_{qd}) \tag{31}$$

Where 0 is a zero matrix. *QRD* stands for QR decomposition. The dimensions of λ, Q_1, Q_2, R_1, zero matrix and Q_{ed} are 12x1, 12x11, 12x1 11x11 and 1x11 and 11x1, respectively.

5.2 Cable Elongation

Since it is assumed the cable is inextensible, the conventional definition of elongation, which is the change in length of cable, cannot be used in the analysis. Instead, the term elongation is defined as the infinitesimal travel distance of cable with respect to an infinitesimal displacement at Joint H. Such infinitesimal travel distance of cable is derived from the off-pulley length of a cable section connected to a pulley, which is similar to that described in Eqns. (18) to (20). The cable elongation in the upward motion of the DT-linkage is

$$\begin{aligned} dL_{12} &= Rd\theta_1 \\ dL_{23} &= -Rd\theta_2 \\ dL_{34} &= R(-d\theta_3 + d\theta_8) \\ dL_{45} &= -Rd\theta_4 \\ dL_{56} &= R(d\theta_5 - d\theta_9) \\ dL_{67} &= -Rd\theta_6 \end{aligned} \tag{32}$$

Where the two subscripts indicate the indices of the pulleys, where the cable section is located in between. dL and $d\theta$ are the infinitesimal displacements of cable and infinite rotation of pulley, respectively. The cable elongation in the downward motion is derived similarly.

Equation (32) relates the cable elongation to the infinitesimal displacement of the generalised coordinates. These generalised coordinates need to be further related to the infinitesimal displacement of Joint H, which is dy_H. The connection between other generalised coordinates and dy_H is derived from the constraint approach, which states that

$$\frac{\partial c}{\partial q_d}\dot{q}_d + \frac{\partial c}{\partial q_i}\dot{q}_i = C_{qd}\dot{q}_d + C_{qi}\dot{q}_i = 0 \tag{33}$$

Where the rate of change of the generalised coordinates $\dot{q}$ terms are the dq terms in this analysis. By solving Eqn. (33), independent generalised coordinate $d\theta_1$ is related to dy_H. The rest of the dependent generalised coordinates $d\theta$ can in turn be related to dy_H through $d\theta_1$. However, Eqn. (33) cannot be solved for an analytical solution due to the over-constrained system. Hence QR decomposition must be used, and the numerical solution is given by

$$dq_d = -R_1^{-1} Q_1^T C_{di} dq_i \tag{34}$$

Where Q_1 and R_1 are the same as the ones given in Eqn. (31). By combining Eqns. (32) and (34), the elongation of cable can be calculated with respect to d_{yH}. The outcomes of Eqns. (30), (26), (27) for cable tension, and Eqns. (32) and (34) for cable elongation are substituted into Eqn. (29) to determine the minimum required stiffness of the cable.

5.3 Numerical Results of Example Cable-Constrained DT-Linkage

The numerical solution of cable tension, actuator input torque and minimum cable stiffness are calculated for the DT-linkage with the same dimension as that on the prototype in [23]. The physical parameters used in the calculation are summarised below in Table 6. The range of actuator input angle θ_1 is 80 to 280 degrees in the analysis, which is slightly smaller than the actual range of 72.54 to 287.45 degrees. The interval of input angle θ_1 is 10 degrees when θ_1 is less than 160 degrees or greater than 210 degrees. To capture the rapid change in cable tension near the singular configuration, the resolution is increased to 2 degrees in between 160 and 210 degrees.

Parameters	Magnitude
$\overline{AO}$ mm	400
v	0.3
r	1.18
Pulley radius R mm	25
External force horizontal F_{Hx} N	0
External force vertical F_{Hy} N	± 8
External moment M_{θ_7} N	0
Max tip deformation d_{yH} mm	5

Tab. 6: Parameters of DT-linkage prototype

In the case where the DT-linkage moves upwards, a negative external force F_{Hy} is applied. The resulting cable tension is presented in Fig. 8. The results for positive F_{Hy} when the DT-linkage moves downwards is identical to Fig. 8.

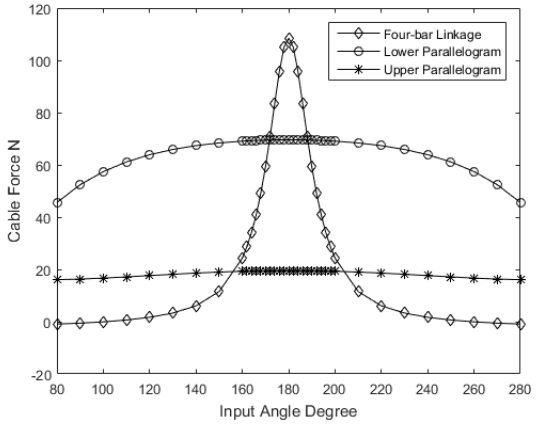

Fig. 8: Cable forces for cable section A under negative load

Fig. 8 indicates that the constraint forces in Loops PL and PU are always positive in their designed directions of motion. The maximum values are 69.59 and 19.52 N for the lower and upper cable loops, respectively. On the other hand, Sections FB encounter changes in direction of constraint force in both directions of motion of the DT-linkage. The changes occur at 110 and 250 degrees, where the constraint force is negative (compression) at smaller than 110 degrees and greater than 250 degrees. However, such negative constraint force does not compromise the

functioning of the cable system. This is because Sections FB are needed only at the singular configuration. In all other configurations, Sections FB are redundant, as the four-bar linkage BCDG is constraining the mechanism. In practice, pre-tension can also be applied to the cable to eliminate the negative regions. The maximum cable tension is observed at the singular configuration, at 108.48 N.

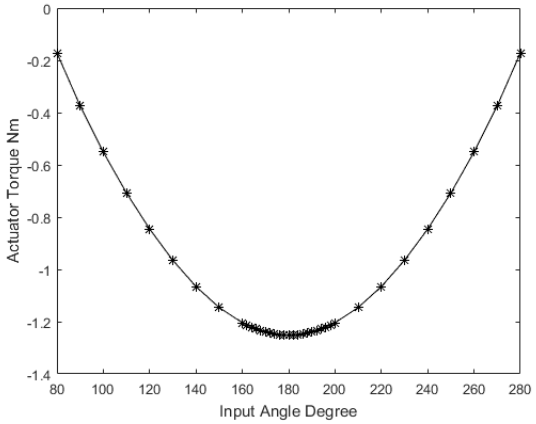

Fig. 9: Actuator input torque under negative load

The actuator input torque τ_1 under negative F_{Hy}, recovered with Eqn. (16) is illustrated in Fig. 9. The maximum input torque required is 1.25 Nm at the singular configuration. The actuator torque under positive F_{Hy} is the same in magnitude but has opposite sign.

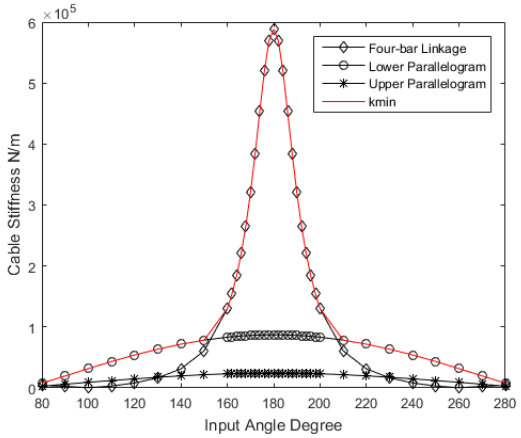

Fig. 10: Minimum required stiffness

The minimum required stiffness with respect to input angle is presented in Fig.10. The black lines with marks are the minimum required stiffness in each of the cable loops, while the red line represents the k_{min} of the cable-constrained DT-linkage as a whole. In the regions near the singular configuration, the stiffness of Sections FB is dominating. On the other hand, when θ_1 is smaller than 150 degrees or greater than 210 degrees, the stiffness of Loop PL determines the overall k_{min}. The maximum value is observed at singular configuration at 5.88e5 N/m, thus the minimum required cable stiffness k_{min} is 5.88e5 N/m.

6 Conclusion

This paper presents the work on a cable-constrained planar RCM linkage. The cable system consists of seven pulleys which form three loops. It provides backlash-free constraints on the planar RCM linkage, which removes

singularity and achieves doubling of ROM (comparing to unconstrained DT-linkage) without expanding the device footprint. In addition it reduces the device footprint taken by the parallelograms on the previous linkage-based prototypes. Analysis based on constraint approach is carried out, leading to analytical solutions of cable force at the singular configuration, as well as numerical solution through QR decomposition at all other configurations. The functioning of cable-constraint system is proven, by observing positive cable force (tension) in cable sections in between all pulley pairs. The minimum required stiffness of cable corresponding to overall stiffness is calculated numerically, where QR decomposition is used twice to solve for the numerical solutions of both cable tension and elongation.

References

[1] R. H. Taylor and D. Stoianovici, "Medical robotics in computer-integrated surgery," *IEEE Transactions on Robotics and Automation*, vol. 19, pp. 765–781, Oct. 2003.

[2] C. H. Kuo and J. S. Dai, "Robotics for minimally invasive surgery: A historical review from the perspective of kinematics," in *Proc. History of Machines and Mechanisms*, (Tainan, Taiwan), pp. 337–354, Nov. 2008.

[3] G. Zong and X. Pei, "Classification and type synthesis of 1-dof remote center of motion mechanisms," *Mechanism and Machine Theory*, vol. 43, pp. 1585–1595, Dec. 2008.

[4] C. Chen and M. Pamieta, "Novel linkage with remote center of motion," in *Proc. 3rd IFToMM International Symposium on Robotics and Mechatronics*, vol. 2, (Singapore), pp. 139–147, Oct. 2013.

[5] M. Ghodoussi, S. E. Butner, and Y. Wang, "Robotic surgery - the transatlantic case," in *Proc. IEEE International Conference on Robotics and Automation (ICRA)*, vol. 2, pp. 1882–1888, 2002.

[6] A. Guerrouad and P. Vidal, "Smos: Stereotaxical microtelemanipulator for ocular surgery," in *Proc. Annual International Conference of the IEEE Engineering in Medicine and Biology Society*, vol. 3, (Seattle, USA), pp. 879–880, Nov. 1989.

[7] E. Hempel, H. Fischer, L. Gumb, T. Höhn, H. Krause, U. Voges, H. Breitwieser, B. Gutmann, J. Durke, M. Bock, and A. Melzer, "An mri-compatible surgical robot for precise radiological interventions," *Computer Aided Surgery*, vol. 8, pp. 180–191, 2003.

[8] A. J. Madhani, G. Niemeyer, and J. K. Salisbury, "The black falcon: a teleoperated surgical instrument for minimally invasive surgery," in *Proc. IEEE/RSJ International Conference on Intelligent Robots and Systems*, vol. 2, (Victoria, British Columbia), pp. 936–944, Oct. 1998.

[9] R. H.Taylor, J. Funda, D. D. Crossman, J. K. Karidis, and D. A. LaRose, "Remote center-of-motion robot for surgery," 1995.

[10] S. J. Blumenkranz and D. J. Rosa, "Manipulator for positioning linkage for robotics surgery," 1995.

[11] M. Feng, Y. Fu, B. Pan, and C. Liu, "Development of a medical robot system for minimally invasive surgery," *The International Journal of Medical Robotics and Computer Assisted Surgery*, vol. 8, pp. 85–96, Mar. 2012.

[12] K. Kim, H. Song, S. Park, J. Lee, and Y. Yoon, "Design and evaluation of a teleoperated surgical manipulator with an additional degree of freedom for laparoscopic surgery," *Advanced Robotics*, vol. 24, pp. 1697–1718, 2010.

[13] W. H. Zhu, S. E. Salcudean, S. Bachmann, and P. Abolmaesumi, "Motion/force/image control of a diagnostic ultrasound robot," in *Proc. IEEE International Conference on Robotics and Automation (ICRA)*, vol. 2, (San Francisco, USA), pp. 1580–1585, Apr. 2000.

[14] D. Stoianovici, L. L. Whitcomb, D. Mazilu, R. H. Taylor, and R. L. Kavoussi, "Remote center of motion robotic system and method," 2004.

[15] M. J. H. Lum, D. C. W. Friedman, G. S. H. King, K. Fodero, R. Leuschke, B. Kannaford, J. Rosen, and M. N. Sinanan, "The revan: Design and validation of a telesurgery system," *The International Journal of Robotics Research*, vol. 28, pp. 1183–1197, 2009.

[16] G. Bai, D. Li, S. Wei, and Q. Liao, "Kinematics and synthesis of a type of mechanisms with multiple remote centers of motion," *Proceedings of the Institution of Mechanical Engineers, Part C: Journal of Mechanical Engineering Science*, vol. 228, no. 18, pp. 3430–3440, 2014.

[17] C.-H. Kuo, J. S. Dai, and P. Dasgupta, "Kinematic design considerations for minimally invasive surgical robots: an overview," *The International Journal of Medical Robotics and Computer Assisted Surgery*, vol. 8, no. 2, pp. 127–145, 2012.

[18] H. Long, Y. Yang, X. Jingjing, and S. Peng, "Type synthesis of 1r1t remote center of motion mechanisms based on pantograph mechanisms," *Journal of Mechanical Design*, vol. 138, no. 1, p. 014501, 2016.

[19] J. Li, Y. Xing, K. Liang, and S. Wang, "Kinematic design of a novel spatial remote center-of-motion mechanism for minimally invasive surgical robot," *Journal of Medical Devices*, vol. 9, no. 1, p. 011003, 2015.

[20] R. R. Solomon and T. Cooper, "Multi-ply strap driver trains for robotic arms," 2007.

[21] G. Haber, M. A. White, R. Autorino, R. F. Escobar, M. D. Kroh, S. Chalikonda, R. Khanna, S. Forest, B. Yang, F. Altunrenda, R. J. Stein, and J. H. Kaouk, "Novel robotic da vinci instruments for laparoendoscopic single-site surgery," *Urology*, vol. 76, pp. 1279–1282, Dec. 2010.

[22] M. Hadavand, A. Mirbagheri, S. Behzadipour, and F. Farahmand, "A novel remote center of motion mechanism for the force-reflective master robot of haptic tele-surgery systems," *The International Journal of Medical Robotics and Computer Assisted Surgery*, vol. 10, no. 2, pp. 129–139, 2014.

[23] S. Liu, C. Chen, B. Chen, and L. Harewood, "Novel linkage with remote centre of motion," in *Proc. 14th IFToMM World Congress*, (Taipei, Taiwan), Oct. 2015.

[24] R. H. Taylor and D. Stoianovici, "Is smaller workspace a limitation for robot performance in laparoscopy?," *The Journal of Urology*, vol. 179, pp. 1138–1143, Mar. 2008.

[25] G. Thomas, T. Cooper, and R. Solomon, "Offset remote center manipulator for robotic surgery," 2009.

[26] M. Muller, "A novel classification of planar four-bar linkages and its application to the mechanical analysis of animal systems," *Philosophical Transaction of the Royal Society B: Biological Sciences*, vol. 351, pp. 689–720, May 1996.

[27] C. Chen, "Power analysis of epicyclic transmissions based on constraints," *Journal of Mechanisms and Robotics*, vol. 4, Nov. 2012.

[28] A. A. Shabana, *Computational Dynamics*. Chichester, UK: Wiley, 2010.